

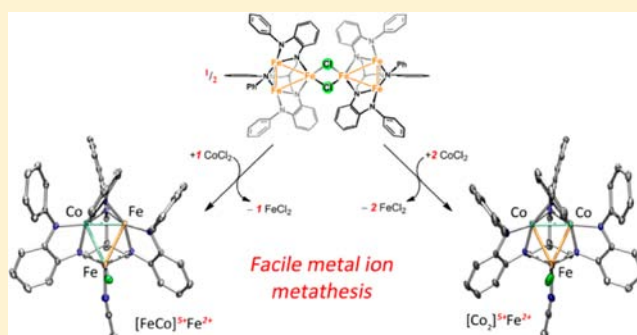
Metal Atom Lability in Polynuclear Complexes

Emily V. Eames, Raúl Hernández Sánchez, and Theodore A. Betley*

Department of Chemistry and Chemical Biology, Harvard University, 12 Oxford Street, Cambridge Massachusetts 02138, United States

Supporting Information

ABSTRACT: The asymmetric oxidation product $[(^{\text{Ph}}\text{L})\text{Fe}_3(\mu\text{-Cl})_2]$ [$^{\text{Ph}}\text{LH}_6 = \text{MeC}(\text{CH}_2\text{NHPH-}o\text{-NHPH})_3$], where each trinuclear core is comprised of an oxidized diiron unit $[\text{Fe}_2]^{5+}$ and an isolated trigonal pyramidal ferrous site, reacts with MCl_2 salts to afford heptanuclear bridged structures of the type $(^{\text{Ph}}\text{L})_2\text{Fe}_6\text{M}(\mu\text{-Cl})_4(\text{thf})_2$, where $\text{M} = \text{Fe}$ or Co . Zero-field, ^{57}Fe Mössbauer analysis revealed the Co resides within the trinuclear core subunits, not at the octahedral, halide-bridged $\text{MCl}_4(\text{thf})_2$ position indicating Co migration into the trinuclear subunits has occurred. Reaction of $[(^{\text{Ph}}\text{L})\text{Fe}_3(\mu\text{-Cl})_2]$ with CoCl_2 (2 or 5 equivalents) followed by precipitation via addition of acetonitrile afforded trinuclear products where one or two irons, respectively, can be substituted within the trinuclear core. Metal atom substitution was verified by ^1H NMR, ^{57}Fe Mossbauer, single crystal X-ray diffraction, X-ray fluorescence, and magnetometry analysis. Spectroscopic analysis revealed that the Co atom(s) substitute(s) into the oxidized dimetal unit ($[\text{M}_2]^{5+}$), while the M^{2+} site remains iron-substituted. Magnetic data acquired for the series are consistent with this analysis revealing the oxidized dimetal unit comprises a strongly coupled $S = 1$ unit ($[\text{FeCo}]^{5+}$) or $S = 1/2$ ($[\text{Co}_2]^{5+}$) that is weakly antiferromagnetically coupled to the high spin ($S = 2$) ferrous site. The kinetic pathway for metal substitution was probed via reaction of $[(^{\text{Ph}}\text{L})\text{Fe}_3(\mu\text{-Cl})_2]$ with isotopically enriched $^{57}\text{FeCl}_2(\text{thf})_2$, the results of which suggest rapid equilibration of ^{57}Fe into both the M^{2+} site and oxidized diiron site, achieving a 1:1 mixture.



I. INTRODUCTION

Polynuclear, heterometallic clusters are employed in nature to facilitate small molecule activation.^{1–3} Two prototypical enzymes that feature heteropolynuclear metal cofactors are the water oxidizing center in photosystem II² and the nitrogen fixing cofactors of nitrogenase.¹ In water oxidation, the presence of Ca within the $\text{Mn}_4\text{O}_4\text{Cl}$ cofactor is critical for oxygen evolution, though the mechanistic role Ca plays is still a topic of debate.⁴ The composition of the nitrogen-reducing cofactor has been observed to contain Fe alone⁵ in a fused cubane structure with an iron–sulfur Fe_8S_9 cluster or heterometallic clusters where a single Fe is replaced with Mo^1 or V^6 in the FeMo and FeV cofactors, respectively. The cofactor composition has been reported to have significant ramifications on the enzymatic chemoselectivity and catalytic efficacy.⁷ The desirable properties afforded by polymetallic assemblies extend beyond enzymatic function, as mixed-metal assemblies have impacted applications in metallurgy, electrochemistry, and heterogeneous catalysis.⁸

Research into the synthesis of abiological, polymetallic clusters is aimed at understanding how metal atom substitution alters the cluster electronic properties and reactivity profiles of the resulting clusters. Synthetic effort targeting polymetallic clusters falls into three general categories: formation using nonselective, self-assembly processes,⁹ reaction of incomplete clusters (e.g., partially formed cubanes) with binary transition

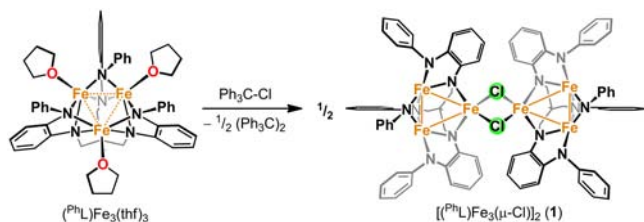
metal or alkaline ions,¹⁰ or using polynucleating ligands that have different elemental binding affinities.¹¹ The selective exchange of transition metals into a polynuclear cluster could be a potential method for the preparation of polymetallic clusters in a systematic fashion, allowing for rigorous study of the electronic property perturbations of the newly formed polymetallic species. In this contribution, we present the metal atom metathesis of cobalt for iron within a preformed, all-iron trinuclear species to afford isostructural bimetallic cluster analogues.

We have observed that low-spin and high-spin iron-based clusters mediate redox processes in two distinct pathways. In the low-spin regime, core-delocalized redox behavior was observed where intracore bonding is enhanced.¹² In contrast, the chemical oxidation of high-spin $(^{\text{Ph}}\text{L})\text{Fe}_3(\text{thf})_3$ ¹³ [$^{\text{Ph}}\text{LH}_6 = \text{MeC}(\text{CH}_2\text{NHPH-}o\text{-NHPH})_3$ binds as a hexadentate, hexaanionic ligand when fully deprotonated] leads to cluster oxidation where the trinuclear core distorts featuring a diiron site as the locus of oxidation $[\text{Fe}_2]^{5+}$, separate from the site of halide capture at a formally +2 iron site (Scheme 1).¹⁴ Oxidation is accompanied by a significant ligand rearrangement to accommodate the distorted core. Typically, such ligand reorganization presents a large energy barrier; thus we

Received: December 7, 2012

Published: April 23, 2013

Scheme 1



proposed that the maximally high-spin formulation of the all-ferrous precursor creates an inherently labile system. In this contribution, we present data to suggest the notion that lability extends beyond ligand reorganization to include the facile exchange of metal atoms out of the polynuclear core.

II. EXPERIMENTAL SECTION

Materials and Methods. All manipulations involving metal complexes were carried out using standard Schlenk line or glovebox techniques under a dinitrogen atmosphere. All glassware was oven-dried for a minimum of 4 h and cooled in an evacuated antechamber prior to use in the drybox. Benzene, diethyl ether, acetonitrile (NCCH₃), and tetrahydrofuran (THF) were dried and deoxygenated on a Glass Contour System (SG Water USA, Nashua, NH) and stored over 4 Å molecular sieves (Strem) prior to use. Benzene-*d*₆, NCCH₃-*d*₃, and THF-*d*₈ were purchased from Cambridge Isotope Laboratories and were degassed and stored over 4 Å molecular sieves prior to use. Solvents were typically tested with a standard purple solution of sodium benzophenone ketyl in THF in order to confirm effective oxygen and moisture removal. MeC(CH₂NHP-*o*-NHPh)₃ (PhL),¹³ (PhL)Fe₃(thf)₃, and [(PhL)Fe₃(μ-Cl)]₂ (1) were prepared following published methods.^{13,14} ⁵⁷Fe powder was purchased from Cambridge Isotope Laboratories and converted to ⁵⁷Fe-enriched FeCl₂ by disproportionation with FeCl₃ following the procedure outlined by Wilkinson.¹⁵ All other reagents were purchased from commercial vendors and used without further purification unless explicitly stated.

Physical Measurements. All of the measurements for the metal complexes except XRF analysis were made under anaerobic conditions. Elemental analyses were performed by Complete Analysis Laboratories, Inc., Parsippany, New Jersey. ¹H NMR spectra were recorded on a Varian Unity/Inova 500B NMR spectrometer with chemical shifts (δ ppm) referenced to residual NMR solvent. UV/visible spectra were recorded on a Varian Cary 50 UV/Visible spectrometer using quartz cuvettes. NIR spectra were recorded on a Perkin Elmer Lambda 750 high-performance UV-vis spectrometer. X-ray fluorescence analyses were recorded on a Bruker Tracer III-SD XRF analyzer with the yellow filter (composition 12 mil Al and 1 mil Ti, passes 12–40 keV), and data were collected on each sample for at least 2 min. Samples for the calibration curve were prepared by grinding together cobalt(II)-chloride hexahydrate and ferrous chloride tetrahydrate. The spectra of pure Fe and Co were each fit to two Voigt lineshapes. The calibration samples were then fit to four Voigt lineshapes, with the areas of each peak varying freely but all other parameters held to the reference values. Fits are substantially poorer if the Kα:Kβ peak area ratios are fixed, though the overall results are unchanged. Quantification was performed using only the Kα peak areas, but there is no difference in result if the Kα and Kβ areas are summed. Fe/Co ratios in samples were determined by fitting using the calibration data and calculating the Fe/Co ratio from the peak area ratios using the linear fit to the calibration curve.

Magnetic measurements were recorded using a Quantum Design MPMS-XL magnetometer. Powdered samples were placed in Lilly #4 gel capsules and thoroughly saturated with melted eicosane wax to prevent particle torquing in the magnetic field. Samples were suspended in the magnetometer using plastic straws. Samples were prepared under a dinitrogen atmosphere in a glovebox. DC magnetic susceptibility data were collected in the temperature range 5–300 K under fields of 0.1, 0.5, 1, and 2 T. Magnetization data were acquired at

1.8–10 K under fields of 1, 2, 3, 4, 5, 6, and 7 T. Susceptibility data were corrected for the diamagnetic contribution of a blank sample consisting of the wax, capsule, and straw at the correct field and temperature. The magnetic susceptibilities were adjusted for diamagnetic contributions using the constitutive corrections from Pascal's constants. The molar magnetic susceptibility (χ_m) was calculated by converting the magnetization (*M*) obtained from the magnetometer to a molar susceptibility using the multiplication factor [molecular weight (MW)]/[sample weight (*m*) × field strength (*H*)]. All samples were checked for ferromagnetic impurities by collecting a field dependence curve at 100 K, and samples were rejected if any deviation from linearity was observed.

Zero-field, ⁵⁷Fe Mössbauer spectra were measured on a constant acceleration spectrometer (SEE Co, Minneapolis, MN) with a Janis SVT-100 cryostat. Isomer shifts are quoted relative to α-Fe foil (<25 μm thick) at room temperature. Samples were prepared using approximately 30 mg of sample suspended in paratone-N oil. Temperatures were controlled using a LakeShore 321 autotuning temperature controller. Temperature variations were no greater than ±10 K, and were generally within ±2 K. Data were analyzed using an in-house package written by E. R. King and modified by E. V. Eames in Igor Pro (Wavemetrics).

Preparation of [(PhL)₂Fe₂(μ-Cl)₄(thf)₂] (2). A chilled (−35 °C) solution of [(PhL)Fe₃(μ-Cl)]₂ (1; 100 mg, 61.3 μmol, 1 equiv) in tetrahydrofuran (15 mL) was added to solid FeCl₂ (8 mg, 63.5 μmol, 1.04 equiv) and stirred for 3 h, allowing the reaction to warm to room temperature. The volatiles were removed under vacuum conditions. Benzene (5 mL) was added with three drops of tetrahydrofuran to the solids, and the resulting solution was filtered through a pipet fitted with filter paper and stored at room temperature. The resulting precipitate was washed with diethyl ether and dried under vacuum conditions. Yield: 60 mg (52%). X-ray quality crystals were grown from a concentrated solution in benzene at room temperature. Anal. Calcd for C₉₀H₈₈Fe₇N₁₂Cl₄O₂: C, 56.82; H, 4.66; N, 8.83. Found: C, 56.57; H, 4.61; N, 8.71.

Preparation of [(PhL)₂Fe₆Co(μ-Cl)₄(thf)₂] (3). A chilled (−35 °C) solution of 1 (60 mg, 37 μmol, 1 equiv) in tetrahydrofuran (15 mL) was added to solid CoCl₂ (4.8 mg, 37 μmol, 1 equiv) and stirred for 3 h, allowing the reaction to warm to room temperature. The volatiles were removed under vacuum conditions. Benzene (5 mL) was added with three drops of tetrahydrofuran to the solids, and the resulting solution was filtered through a pipet fitted with filter paper and stored at room temperature. The resulting precipitate was washed with benzene and dried under vacuum conditions. Yield: 35 mg (51%). X-ray quality crystals were grown from a concentrated solution in benzene at room temperature. Anal. Calcd for C₉₀H₈₈Fe₆CoN₁₂Cl₄O₂: C, 56.73; H, 4.65; N, 8.82. Found: C, 56.69; H, 4.58; N, 8.75.

Preparation of [(PhL)Fe₂CoCl(NCCH₃)] (4). A solution of 1 (130 mg, 80 μmol, 1 equiv) in thawing tetrahydrofuran (20 mL) was added to solid CoCl₂ (21.2 mg, 164 μmol, 2.06 equiv) and stirred for 3 h, allowing the reaction to warm to room temperature. The volatiles were removed under vacuum conditions. Acetonitrile (2 mL) was added, briefly dissolving the solid and rapidly precipitating a crystalline product. The crystals were collected on a fritted glass funnel and washed with acetonitrile (3 mL), then dissolved in benzene and filtered to remove any insoluble material. The volatiles were removed under vacuum conditions, and four drops of tetrahydrofuran were added, followed by acetonitrile (2 mL). The product, which precipitated from acetonitrile, was collected on a fritted glass funnel and washed with more acetonitrile, then dried under vacuum conditions. Recrystallized yield: 58 mg (42%). X-ray quality crystals were grown from a concentrated solution in acetonitrile at room temperature. ¹H NMR (C₆D₆ with 3 drops NCCH₃-*d*₃, 500 MHz, δ, ppm): 54, 48, 46, 45, 41, 23, 17, 16, 11, 5, 2, −2, −5, −14, −29, −39, −72, −77, −90. Anal. Calcd for C₄₃H₃₉Fe₂CoN₇Cl: C, 60.06; H, 4.57; N, 11.40. Found: C, 59.96; H, 4.59; N, 11.42.

Preparation of [(PhL)FeCo₂Cl(NCCH₃)] (5). A solution of 1 (140 mg, 86 μmol, 1 equiv) in thawing tetrahydrofuran (20 mL) was added to solid CoCl₂ (57.1 mg, 443 μmol, 5.1 equiv) and stirred for 3 h, allowing the reaction to warm to room temperature. The volatiles were

removed under vacuum conditions. Acetonitrile (2 mL) was added, briefly dissolving the solid and rapidly precipitating a crystalline product. The crystals were collected on a fritted glass funnel and washed with acetonitrile (3 mL), then dissolved in benzene and filtered to remove any insoluble material. The volatiles were removed under vacuum conditions, and four drops of tetrahydrofuran were added, followed by acetonitrile (2 mL). The product, which precipitated from acetonitrile, was collected on a fritted glass funnel and washed with more acetonitrile, then dried under vacuum conditions. Recrystallized yield: 60.3 mg (41%). X-ray quality crystals were grown from a concentrated filtered solution in acetonitrile at room temperature. ^1H NMR (C_6D_6 with three drops NCCH_3 - d_3 , 500 MHz, δ , ppm): 48, 46, 30, 28, 26, 24, 17, 15, 11, 10, 5.5, -2, -4, -8, -16, -19, -29, -39, -42, -56, -72. Anal. Calcd for $\text{C}_{43}\text{H}_{39}\text{FeCo}_2\text{N}_7\text{Cl}$: C, 59.85; H, 4.55; N, 11.36. Found: C, 59.75; H, 4.66; N, 11.28.

Preparation of $[(^{\text{Ph}}\text{L})\text{FeCo}_2(\mu\text{-Cl})_2]$ (6). A solution of **1** (140 μmol , 86 μmol , 1 equiv) in thawing tetrahydrofuran (20 mL) was added to solid CoCl_2 (57.1 mg, 443 μmol , 5.1 equiv) and stirred for 5 h, allowing the reaction to warm to room temperature. The volatiles were removed under vacuum conditions. Acetonitrile (2 mL) was added, briefly dissolving the solid, and rapidly precipitated a crystalline product. The crystals were collected on a fritted glass funnel and washed with acetonitrile (3 mL), then dissolved in benzene and filtered to remove any insoluble material. The volatiles were removed under vacuum conditions, followed by dissolution in benzene (5 mL), and the solution was stored overnight. The crystalline material was collected on a fritted glass funnel and washed with benzene, then dried under vacuum conditions. Recrystallized yield: 52 mg (37%). X-ray quality crystals were grown from a concentrated solution in benzene at room temperature. Anal. Calcd for $\text{C}_{41}\text{H}_{36}\text{FeCo}_2\text{N}_6\text{Cl}$: C, 59.91; H, 4.41; N, 10.22. Found: C, 59.94; H, 4.47; N, 10.08.

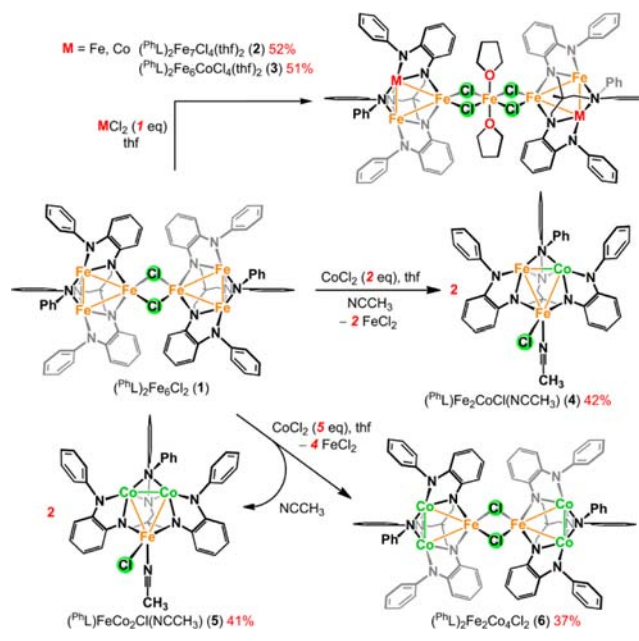
Preparation of $(^{\text{Ph}}\text{L})\text{Fe}_3\text{Cl}(\text{NCCCH}_3)$ (7). To a solution of **1** (50 μmol , 31 μmol) in benzene (5 mL) was added 25 drops of acetonitrile. The solution was filtered and the volatiles removed under vacuum conditions. No crystals of this material were ever obtained, despite numerous attempts. Yield: 51 mg (97%). ^1H NMR (C_6D_6 with 3 drops NCCH_3 - d_3 , 500 MHz, δ , ppm): 53, 36, 33, 28, 19, 13.5, 12, 6, -16, -47, -80, -98. Anal. Calcd for $\text{C}_{43}\text{H}_{39}\text{Fe}_3\text{N}_7\text{Cl}$: C, 60.28; H, 4.59; N, 11.44. Found: C, 60.26; H, 4.54; N, 11.42.

^{57}Fe Exchange Experiments. Degenerative exchange of ^{57}Fe -enriched $\text{FeCl}_2(\text{thf})_2$ was observed by zero-field, ^{57}Fe Mössbauer spectroscopy. Enriched $\text{FeCl}_2(\text{thf})_2$ (2.5 mg, 0.5 equiv) was dissolved in tetrahydrofuran (2 mL) with stirring, cooled to -35°C in the glovebox freezer, and added to **1** (30 mg, 18.4 μmol) frozen in 5 mL of tetrahydrofuran. This experiment was performed in triplicate, and the resulting solutions were filtered through a pipet fitted with filter paper and evacuated to dryness (with constant stirring) under vacuum conditions after 0, 2, and 15 h had elapsed. Mössbauer samples were prepared from the collected solids (~ 15 mg).

III. RESULTS AND DISCUSSION

While exploring the incorporation of the oxidized trinuclear species $(^{\text{Ph}}\text{L})\text{Fe}_3\text{X}$ unit into larger assemblies, we observed the propensity for metal atom substitution within the core. For example, stirring $[(^{\text{Ph}}\text{L})\text{Fe}_3(\mu\text{-Cl})_2]$ (**1**) with FeCl_2 or CoCl_2 in tetrahydrofuran afforded new complexes that could be crystallized from benzene yielding $(^{\text{Ph}}\text{L})\text{Fe}_7(\mu\text{-Cl})_4(\text{thf})_2$ (**2**) and $(^{\text{Ph}}\text{L})\text{Fe}_6\text{Co}(\mu\text{-Cl})_4(\text{thf})_2$ (**3**), respectively (Scheme 2). The solid-state molecular structures for **2** and **3** both feature two trinuclear cores bridged by a single metal atom via four bridging chloride ligands (see Figure 1c for a representative molecular structure of **2** and Figures S2 and S3).¹⁵ Zero-field, ^{57}Fe Mössbauer analysis of **2** was fit to four quadrupole doublets (δ , $|\Delta E_Q|$ (mm/s), Figure 1a): two quadrupole doublets for $[\text{Fe}_2]^{3+}$ (0.28, 2.38; 0.17, 2.67; 54% of the total Fe), the ferrous site in the trinuclear subunit (0.72, 1.32; Fe^{2+} ; 29%), and the bridge position (1.18, 2.37; $\text{FeCl}_4(\text{thf})_2$; 17%), in

Scheme 2



nearly the expected ratio of 4:2:1, and the metrical parameters for the trinuclear cores match well with those reported for **1**.¹⁴ For complex **3**, three quadrupole doublets are present with the following metrical parameters (δ , $|\Delta E_Q|$ (mm/s)): 0.21, 2.69 (38.9%); 0.73, 1.39 (38.9%); and 1.16, 2.35 (22%), which coincide with spectral features for the $[\text{Fe}_2]^{3+}$, Fe^{2+} , and $\text{FeCl}_4(\text{thf})_2$ sites, respectively, in **2** (see Figure 1b). If the Co atom occupied the tetrachloro-bridge position $\text{MCl}_4(\text{thf})_2$, we would anticipate the spectral features for the trinuclear subunits to be unchanged and no spectral features for the $\text{MCl}_4(\text{thf})_2$ site. However, the data are consistent with two iron atoms in the trinuclear cores and iron, not cobalt, residing in the $\text{MCl}_4(\text{thf})_2$ site, suggesting Co atom migration into the trinuclear subunits has occurred. This metal atom substitution is striking in that a minimum of four Fe–N bonds must be broken concomitant with the formation of four Co–N bonds.

To explore this substitution reaction further, we investigated the reactivity of complex **1** with two or five equivalents of CoCl_2 (giving Fe/Co ratios of 3:1 and 3:2.5, respectively) in tetrahydrofuran for 3 h at room temperature. Following removal of the volatiles *in vacuo*, acetonitrile was added to the solid. The solids briefly dissolved and rapidly precipitated a fraction of the material as crystals. The crystallized material was collected on a fritted glass funnel and washed with acetonitrile. The collected product was recrystallized from a mixture of tetrahydrofuran and acetonitrile at room temperature. The reaction products obtained from these two reactions are consistent with the following compositions: $(^{\text{Ph}}\text{L})\text{Fe}_2\text{CoCl}(\text{NCCCH}_3)$ (**4**) from the reaction of **1** with two equivalents of CoCl_2 , and $(^{\text{Ph}}\text{L})\text{Co}_2\text{FeCl}(\text{NCCCH}_3)$ (**5**) from the reaction of **1** with five equivalents of CoCl_2 (see Scheme 2). Excess CoCl_2 is used in the latter case to ensure full substitution during the time scale of the reaction, while in the former reaction precisely one equivalent of CoCl_2 per equivalent of $(^{\text{Ph}}\text{L})\text{Fe}_3\text{Cl}$ is used to prevent oversubstitution to form **5**. Without the addition of extra acetonitrile during crystallization from benzene, the halide-bridged species was obtained $[(^{\text{Ph}}\text{L})\text{Co}_2\text{Fe}(\mu\text{-Cl})_2]$ (**6**) from the reaction with excess CoCl_2 (Figure 2c). Although the complexes **4–6** feature paramagnetically shifted ^1H NMR, the

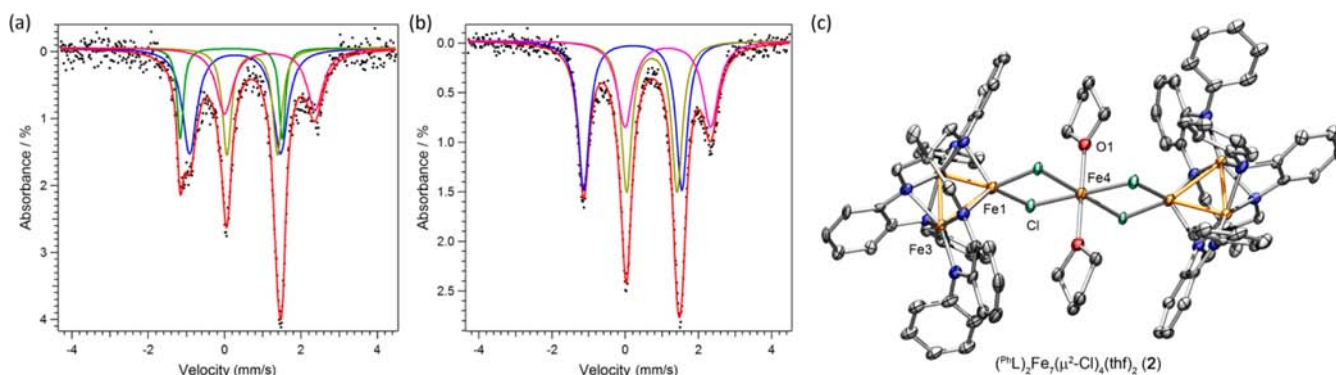


Figure 1. Zero-field ^{57}Fe Mössbauer spectrum obtained at 90 K and spectral fits (δ , $|\Delta E_Q|$ (mm/s)) for (a) $(\text{PhL})_2\text{Fe}_7(\mu\text{-Cl})_4(\text{thf})_2$ (2; (blue, 28.7%) 0.28, 2.38; (green, 24.9%) 0.17, 2.67; (gold, 29%) 0.72, 1.32; (pink, 17.4%) 1.18, 2.37); (b) $(\text{PhL})_2\text{Fe}_6\text{Co}(\mu\text{-Cl})_4(\text{thf})_2$ (3; (blue, 38.9%) 0.21, 2.69; (green, 38.9%) 0.73, 1.39; (gold, 22.3%) 1.16, 2.35). Solid-state structures for $(\text{PhL})_2\text{Fe}_7(\mu\text{-Cl})_4(\text{thf})_2$ (2) with the thermal ellipsoids set at the 50% probability level (hydrogen atoms, and solvent molecules omitted for clarity; Fe, orange; C, gray; N, blue; O, red; Cl, green).

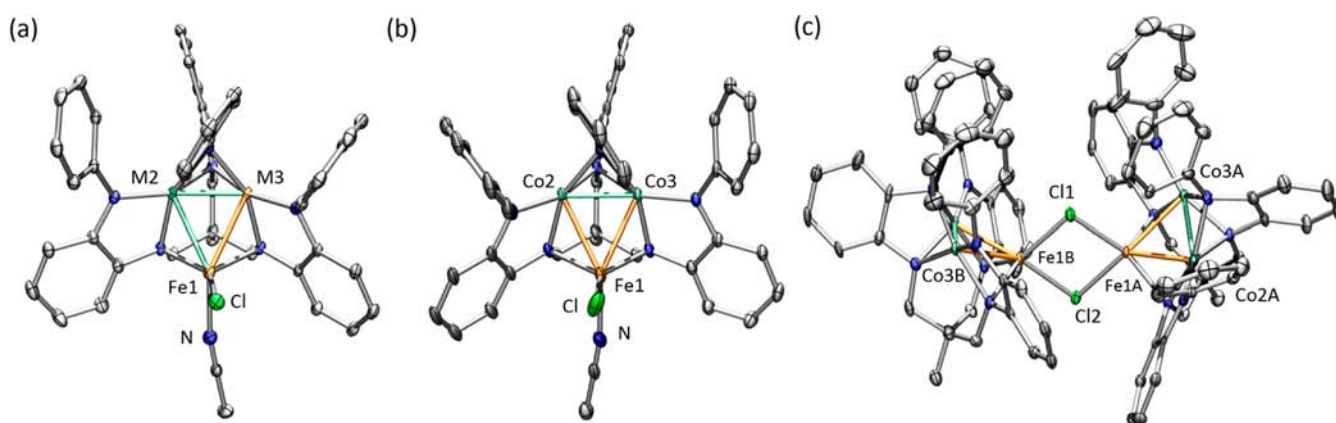


Figure 2. Solid-state structures for (a) $(\text{PhL})\text{M1M2FeCl}(\text{NCCH}_3)$ (4), (b) $(\text{PhL})\text{FeCo}_2\text{Cl}(\text{NCCH}_3)$ (5), and (c) $[(\text{PhL})\text{FeCo}_2(\mu\text{-Cl})]_2$ (6) with the thermal ellipsoids set at the 50% probability level (hydrogen atoms and solvent molecules omitted for clarity; Fe, orange; Co, aquamarine; C, gray; N, blue; O, red; Cl, green). Bond lengths (Å) for 4: Fe1–M2, 2.5391(7); Fe1–M3, 2.5493(8); M2–M3, 2.2934(8); Fe1–Cl, 2.3393(9); Fe1–N_{ACN}, 2.134(3). For 5: Fe1–Co2, 2.5253(6); Fe1–Co3, 2.5348(6); Co2–Co3, 2.2971(5); Fe1–Cl, 2.2348(9); Fe1–N_{ACN}, 2.129(3). For 6: Fe1A–Co2A, 2.5120(14); Fe1A–Co3A, 2.5319(14); Co2A–Co3A, 2.2860(13); Fe1A–Cl1, 2.349(2); Fe1A–Cl2, 2.441(2); Fe1–Fe1, 3.4474(14); Fe1B–Co2B, 2.5009(14); Fe1B–Co3B, 2.5334(14); Co2B–Co3B, 2.2862(14); Fe1B–Cl1, 2.349(2); Fe1B–Cl2, 2.428(2); Fe1–Fe1, 3.4474(14).

spectra are diagnostic and distinguishable (see Figure S18). The spectra for the acetonitrile adducts 4 and 5 are distinct from each other, as well as $(\text{PhL})\text{Fe}_3\text{Cl}(\text{NCCH}_3)$ (7), prepared by the addition of acetonitrile to 1, suggesting 4 and 5 are distinct molecular species with integer Fe/Co ratios, rather than a mixture of substitution products. The evolution of FeCl_2 as an acetonitrile solvate was observed by analysis of the reaction supernatant by ^{57}Fe Mössbauer spectroscopy (δ , $|\Delta E_Q|$ (mm/s): 1.24, 2.16), which matches the metrical parameters for $\text{FeCl}_2(\text{NCCH}_3)_2$ prepared independently (Figure S12).¹⁷

The molecular structures of the reaction products 4–6 were obtained by single crystal X-ray diffraction analysis (see Figure 2). For the acetonitrile-bound, trinuclear complexes 4 and 5, the molecular structures are analogous to the previously described oxidized trinuclear complex $(\text{PhL})\text{Fe}_3\text{Cl}(\text{py})$,¹⁴ maintaining the overall (PhL) coordination mode. The molecular structures feature two metal sites in an intermediate geometry between square planar and tetrahedral (M2 and M3 in Figure 2a) and one metal in a trigonal, monopyramidal geometry (neglecting M–M interactions) bound by chloride, acetonitrile, and two anilide ligands (Fe1 in Figure 2a). As Fe and Co are indistinguishable by X-ray diffraction, the data for complex 4 was refined with an equal population of Co and Fe

in the M2 and M3 positions, whereas the data for 5 were refined with Co exclusively in the dinuclear $[\text{M}_2]^{5+}$ unit. The four-coordinate sites (M2, M3) are each bound to four ligand anilide ligands and feature a close M–M contact (M2–M3, 2.2934(8) Å in 4, Co2–Co3, 2.2971(5) Å in 5) in the axial site. The two remaining M–M contacts between the dinuclear $[\text{M}_2]^{5+}$ unit and the trigonal pyramidal site are shorter compared to M–M separation observed in $(\text{PhL})\text{Fe}_3\text{Cl}(\text{py})$ (data compiled in Table 1), although the solvent ligands are bound in different positions.¹⁴ In $(\text{PhL})\text{Fe}_3\text{Cl}(\text{py})$, the pyridine ligand completes the trigonal plane of Fe1, whereas this

Table 1. Selected Bond Distances

	M1	M1–M2	M2	M1–M3	M3	M2–M3
1	Fe	2.5889(5)	Fe	2.5801(5)	Fe	2.3410(5)
6	Fe _A	2.512(1)	Co _A	2.532(1)	Co _A	2.286(1)
	Fe _B	2.501(1)	Co _B	2.533(1)	Co _B	2.286(1)
Fe_3Cl^a	Fe	2.7303(8)	Fe	2.6534(8)	Fe	2.2955(8)
4	Fe	2.5391(7)	M1	2.5493(8)	M2	2.2934(8)
5	Fe	2.5253(6)	Co	2.5348(6)	Co	2.2971(5)

^a $(\text{PhL})\text{Fe}_3\text{Cl}(\text{py})$.¹⁴

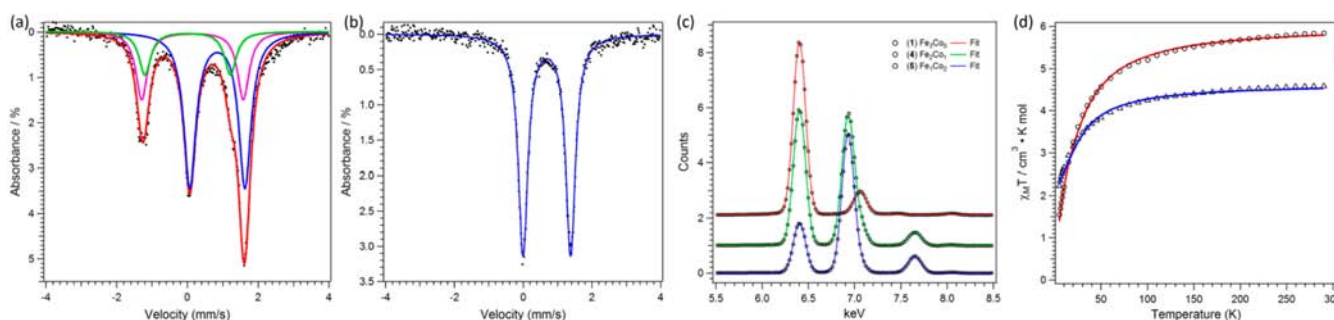


Figure 3. Zero-field ^{57}Fe Mössbauer spectrum obtained at 90 K and spectral fits (δ , $|\Delta E_Q|$ (mm/s)) for (a) $(^{\text{PhL}}\text{Fe}_2\text{CoCl}(\text{NCCH}_3)_4$ (**4**; component 1 (blue): 0.83, 1.41, 56.7%; component 2 (green): -0.01 , 2.36, 22.1%; component 3 (magenta): 0.21, 2.92, 21.1%); (b) $[(^{\text{PhL}}\text{Co}_2\text{Fe}(\mu\text{-Cl}))_2$ (**6**; 0.69, 1.38). (c) X-ray fluorescence spectra (data black circles, fits represented as lines): of **1** (red), **4** (green), **6** (blue). (d) Variable-temperature magnetic susceptibility data for **4** (circles) and **5** (triangles) collected in an applied dc field of 0.1 T. Solid lines represent fits to the data as described in the text.

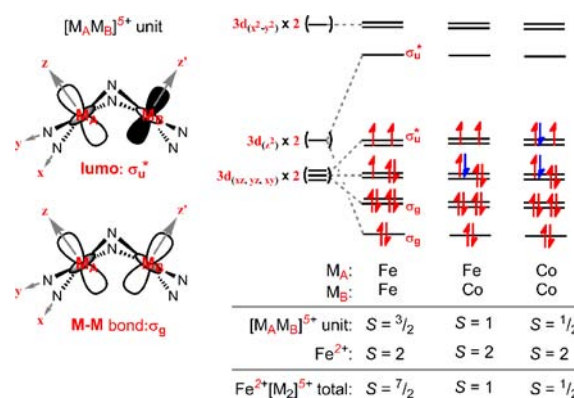
position is occupied by Cl in **4** and **5** which may contribute to some of the trinuclear core distortion observed.

The chloride-bridged complex **6** maintains the connectivity present in its all-iron precursor **1**, providing the best comparison to illustrate the intracore distortions resulting from substitution of iron by cobalt. All three M–M interactions are contracted for the mixed-metal cluster **6** as compared to the metrics found in the all-iron complex **1** (see Table 1). As with the tri-iron congeners, the bond metrics within the $(^{\text{PhL}})$ ligand *o*-phenylenediamide units are consistent with the closed-shell dianion state (see Tables S3–S7), indicating ligand-redox participation is not involved.¹⁸

The zero-field, ^{57}Fe Mössbauer spectra for complexes **4**, **6**, and **7** obtained at 90 K are shown in Figures 3a,b and S11, respectively. Like **1** and the pyridine bound congener $(^{\text{PhL}})\text{Fe}_3\text{Cl}(\text{py})$, the spectrum of **7** features three distinct quadrupole doublets (δ , $|\Delta E_Q|$ (mm/s): 0.71, 1.27, 33.3%; 0.31, 2.48, 33.3%; 0.19, 2.68, 33.3%). The two low-velocity doublets correspond to the iron sites within the oxidized dinuclear unit $[\text{Fe}_2]^{5+}$, while the high-velocity doublet corresponds to the Fe^{2+} pyramidal site. The spectrum for **4** (Figure 3a) shows little perturbation in the metrical parameters (δ , $|\Delta E_Q|$ (mm/s): 0.83, 1.41, 56.7%; -0.01 , 2.36, 22.1%; 0.21, 2.92, 21.1%), except the ratio of high-velocity to low-velocity doublets has changed from almost 1:2 in **7** to 1.3:1 in **4**, signifying the Co substitution is occurring within the oxidized dinuclear unit ($[\text{M}_2]^{5+}$) rather than the M^{2+} site. The spectrum for **6** (Figure 3b) shows complete substitution of both iron atoms by cobalt within the oxidized dinuclear subunit $[\text{M}_2]^{5+}$, leaving only a single quadrupole doublet observed with metrical parameters consistent with the Fe^{2+} site (δ , $|\Delta E_Q|$ (mm/s): 0.69, 1.38). The composition suggested by the Mössbauer analysis was corroborated by X-ray fluorescence analysis. The superposition of Fe and Co $K\alpha$ and $K\beta$ emission lines of crystalline samples for complexes **3**, **4**, and **6** suggest Fe/Co ratios of 6:1, 2:1, and 1:2 (see Figures 3c and S13–S17).

As previously reported, magnetic data acquired for the all-iron oxidation product **1** revealed that the oxidized diiron unit $[\text{Fe}_2]^{5+}$ is comprised of a strongly coupled $S = 3/2$ unit that is weakly ferromagnetically coupled to the high spin ($S = 2$) ferrous site, giving an overall $S = 7/2$ ground state for the trinuclear unit. The close M–M separation within the oxidized dimetal unit $[\text{M}_2]^{5+}$ suggests significant M–M orbital overlap, dictated by the orbital overlap permitted for two edge-sharing square planar ions (Scheme 3).¹⁴ For two Fe atoms comprising the $[\text{M}_2]^{5+}$ unit, population of the 11 valence electrons into this

Scheme 3. Frontier Molecular Orbital Interactions of $[\text{M}_A\text{M}_B]^{5+}$ Unit in **1**, **4**, and **5**



manifold in a quartet configuration prevented population of $(\text{M}-\text{N})_{\sigma^*}$ and $(\text{M}-\text{M})_{\sigma^*}$ (z^2 based) interactions, providing a stabilizing interaction (via M–M bonding) within the oxidized dinuclear unit. With complexes **3**–**6**, substitution of Co for Fe within the oxidized dinuclear unit does not structurally perturb the trinuclear core (*vide supra*) as to suggest reconfiguration of these orbital interactions. Thus, for complex **4** which features a $[\text{FeCo}]^{5+}$ dinuclear unit, we would anticipate a triplet formulation for $[\text{M}_A\text{M}_B]^{5+}$, as the number of valence electrons in the orbital manifold has increased to 12. For complexes **5** and **6**, we would anticipate a doublet configuration for the 13 electron $[\text{Co}_2]^{5+}$ subunit.

To probe the magnetic behavior of complexes **4** and **5** further, variable temperature dc susceptibility data were collected in the temperature range of 5–300 K (Figure 3d). In the case of **4**, $\chi_M T$ decreases from a value of 5.78 $\text{cm}^3 \text{K mol}^{-1}$ at 300 K to a minimum value of 1.55 $\text{cm}^3 \text{K mol}^{-1}$ at 5 K (see Figure 3d). Below 50 K, the data undergo a downturn, likely the result of Zeeman and zero-field splitting. In the case of **5**, $\chi_M T$ decreases from a value of 4.53 $\text{cm}^3 \text{K mol}^{-1}$ at 300 K to a minimum value of 2.23 $\text{cm}^3 \text{K mol}^{-1}$ at 5 K (see Figure 3d).

The foregoing Mössbauer analysis suggests iron uniquely resides in the M^{2+} site of the trinuclear core following Co substitution; thus we modeled the magnetic data using the two-spin Hamiltonian shown below, where $S_1 = 2$ for the ferrous unit and S_2 represents the mixed-valent dinuclear unit spin.

$$\hat{H} = -2J(S_1 S_2) + \sum D_i S_i^2 + g\mu_B \mathbf{S} \cdot \mathbf{B}$$

Following the orbital analysis presented above, the spin state of the oxidized dinuclear $[M_2]^{5+}$ unit S_2 was modeled as a triplet for the $[\text{FeCo}]^{5+}$ unit in **4** and as a doublet for the $[\text{Co}_2]^{5+}$ unit in **5**. The corresponding simulation using the program MAGPACK¹⁹ that best reproduces the susceptibility and reduced magnetization data (see Figures S19–22) affords parameters of $J = -4.25 \text{ cm}^{-1}$, $D_1 = 5.25 \text{ cm}^{-1}$, $D_2 = -20 \text{ cm}^{-1}$, and $g = 2.46$ for complex **4** and $J = -6.25 \text{ cm}^{-1}$, $D_1 = 2.5 \text{ cm}^{-1}$, and $g = 2.35$ for complex **5**. Unlike the all-iron oxidized clusters,¹⁴ substitution of Co into the oxidized dinuclear unit is best modeled as weak antiferromagnetic coupling between the ferrous site and the oxidized dinuclear unit giving rise to $S = 1$ and $S = 1/2$ ground states for complexes **4** and **5**, respectively.

With the compositions for the metal atom substitution reactions confirmed by a variety of spectroscopic techniques, we sought to probe how the metal substitution occurs kinetically. While a myriad of routes may be possible for the CoCl_2 salt to engage the $(^{\text{Ph}}\text{L})\text{Fe}_3\text{Cl}(\text{thf})$ core formed in situ, we propose two such possibilities for consideration: Formation of an extended core (similar to heptanuclear products **2** and **3**), followed by metathesis of Fe^{2+} for cobalt. Subsequent rearrangement of the trinuclear core with respect to the $(^{\text{Ph}}\text{L})$ ligand would position the Co within the oxidized dinuclear site. An alternative pathway could involve CoCl_2 association to the exposed axial face of either of the distorted square planar Fe sites within the oxidized dinuclear core and direct metal atom metathesis occurs into that position. To probe these possibilities we investigated the reaction of complex **1** with ^{57}Fe -labeled $^{57}\text{FeCl}_2(\text{thf})_2$ to produce heptanuclear **2** in tetrahydrofuran at room temperature. The reaction was evacuated to dryness and the ^{57}Fe Mössbauer spectra recorded after stirring times of 0.5, 2.5, and 15 h (see Figures S21–S23). After 30 min of reaction time, both the M^{2+} site and oxidized dinuclear unit are equally enriched with ^{57}Fe , with that ratio remaining fairly constant even at 15 h. Thus, for degenerative exchange of iron within **2**, each site is accessible, but accumulation in the oxidized $[\text{Fe}_2]^{5+}$ to achieve the statistical distribution expected is not observed.

IV. CONCLUSIONS

The ligand reorganization that occurs following oxidation of the high-spin cluster $(^{\text{Ph}}\text{L})\text{Fe}_3(\text{thf})_3$ suggests an inherent lability between the polyanilide framework and trinuclear core. That observation led us to examine whether metal atom substitution within these open-shell complexes could be another manifestation of that metastability. The foregoing analysis, based on crystallographic, magnetic, and Mössbauer spectral data suggests metal atom metathesis from within polynuclear complexes is possible while maintaining the overall morphology of the cluster. Moreover, the $S = 3/2$ $[\text{Fe}_2]^{5+}$ unit in **1**, despite its apparently strong Fe–Fe bonding interaction (certainly strongest within the polynuclear core of **1**), is where metal substitution occurs. Substitution of cobalt for iron within this framework does not introduce strain into the cluster, as the two metals possess nearly identical covalent radii. However, the striking result is how facile the substitution occurs within a preformed cluster to give well-defined bimetallic products. Research is currently underway to determine the generality of this reaction type and establish alternative synthetic pathways to achieve polymetallic clusters of this type.

■ ASSOCIATED CONTENT

Supporting Information

Experimental procedures and spectral data for **2–6**; selected crystallographic data and bond lengths for **2–6**; CIF file for **2–6**. This material is available free of charge via the Internet at <http://pubs.acs.org>.

■ AUTHOR INFORMATION

Corresponding Author

*E-mail: betley@chemistry.harvard.edu.

Notes

The authors declare no competing financial interest.

■ ACKNOWLEDGMENTS

The authors thank Harvard University and NIH (GM 098395) for financial support, Prof. R. H. Holm for the generous use of his Mössbauer spectrometer, the George W. Merck Fellowship (T.A.B.), the CONACYT and Fundación México en Harvard A. C. (R.H.S.), and the Harvard University Center for the Environment for funding (E.V.E.).

■ REFERENCES

- (1) Nitrogenase: (a) Howard, J. B.; Rees, D. C. *Chem. Rev.* **1996**, *96*, 2965. (b) Burgess, B. K.; Lowe, D. J. *Chem. Rev.* **1996**, *96*, 2983. (c) Dos Santos, P. C.; Igarashi, R. Y.; Lee, H.-I.; Hoffman, B. M.; Seefeldt, L. C.; Dean, D. R. *Acc. Chem. Res.* **2005**, *38*, 208. (d) Hoffman, B. M.; Dean, D. R.; Seefeldt, L. C. *Acc. Chem. Res.* **2009**, *42*, 609.
- (2) Photosystem II: (a) Nugent, J. *Biochim. Biophys. Acta* **2001**, *1503*, 1. (b) Ferreira, K. N.; Iverson, T. M.; Maghlaoui, K.; Barber, J.; Iwata, S. *Science* **2004**, *303*, 1831. (c) Iwata, S.; Barber, J. *Curr. Opin. Struct. Biol.* **2004**, *14*, 447.
- (3) Mn/Fe Ribonucleotide reductase: (a) Jiang, W.; Yun, D.; Saleh, L.; Barr, E. W.; Xing, G.; Hoffart, L. M.; Maslak, M.-A.; Krebs, C.; Bollinger, J. M., Jr. *Science* **2007**, *316*, 1188. (b) Jiang, W.; Hoffart, L. M.; Krebs, C.; Bollinger, J. M., Jr. *Biochemistry* **2007**, *46*, 8709.
- (4) (a) Ghanotakis, D. F.; Babcock, G. T.; Yocum, C. F. *FEBS* **1984**, *167*, 127. (b) Krieger, A.; Weis, E. *Photosynth. Res.* **1993**, *37*, 117. (c) Renger, C. *Biochim. Biophys. Acta* **2001**, *1503*, 210. (d) McEvoy, J. P.; Brudvig, G. W. *Chem. Rev.* **2006**, *106*, 4455. (e) Siegbahn, P. E. M. *Inorg. Chem.* **2008**, *47*, 1779.
- (5) (a) Joerger, R. D.; Jacobson, M. R.; Premakumar, R.; Wolfinger, E. D.; Bishop, P. E. *J. Bacteriol.* **1989**, *171*, 1075. (b) Schüdderkopf, K.; Hennecke, S.; Liese, U.; Kutsch, M.; Klipp, W. *Mol. Microbiol.* **1993**, *8*, 673. (c) Zinoni, F.; Robson, R. M.; Robson, R. L. *Biochim. Biophys. Acta* **1993**, *1174*, 83.
- (6) (a) Joerger, R. D.; Loveless, T. M.; Pau, R. N.; Mitchenall, L. A.; Simon, B. H.; Bishop, P. E. *J. Bacteriol.* **1990**, *172*, 3400. (b) Robson, R. L.; Woodley, P. R.; Pau, R. N.; Eady, R. R. *EMBO J.* **1989**, *8*, 1217. (c) Theil, T. *J. Bacteriol.* **1993**, *175*, 6276.
- (7) (a) Lee, C. C.; Hu, Y.; Ribbe, M. W. *Science* **2010**, *329*, 642. (b) Hu, Y.; Lee, C. C.; Ribbe, M. W. *Dalton Trans.* **2012**, *41*, 1118.
- (8) (a) Preetz, W.; Harder, K. Z. *Anorg. Allg. Chem.* **1991**, *597*, 163. (b) Rodriguez, J. A.; Goodman, D. W. *Science* **1992**, *257*, 897. (c) Brückner, P.; Peters, G.; Preetz, W. Z. *Anorg. Allg. Chem.* **1994**, *620*, 1669. (d) Naumov, N. G.; Brylev, K. A.; Mironov, Y. V.; Virovets, A. V.; Fenske, D.; Fedorov, V. E. *Polyhedron* **2004**, *23*, 599.
- (9) Tulsky, E. G.; Long, J. R. *Inorg. Chem.* **2001**, *40*, 6990.
- (10) (a) Hernandez-Molina, R.; Sokolov, M. N.; Sykes, A. G. *Acc. Chem. Res.* **2001**, *34*, 223. (b) Clerac, R.; Cotton, F. A.; Dunbar, K. R.; Murillo, C. A.; Wang, X. *Inorg. Chem.* **2001**, *40*, 420. (c) Rao, P. V.; Holm, R. H. *Chem. Rev.* **2004**, *104*, 527. (g) Lee, S. C.; Holm, R. H. *Chem. Rev.* **2004**, *104*, 1135. (d) Nippe, M.; Berry, J. F. *J. Am. Chem. Soc.* **2007**, *129*, 12684. (e) Nippe, M.; Victor, E.; Berry, J. F. *Eur. J. Inorg. Chem.* **2008**, 5569. (f) Kanady, J. S.; Tsui, E. Y.; Day, M. W.; Agapie, T. *Science* **2011**, *333*, 733.

(11) (a) Pilkington, N. H.; Robson, R. *Aust. J. Chem.* **1970**, *23*, 2225. (b) Beissel, T.; Birkelbach, F.; Bill, E.; Glaser, T.; Kesting, F.; Krebs, C.; Weyhermüller, T.; Wieghardt, K.; Butzlaff, C.; Trautwein, A. X. *J. Am. Chem. Soc.* **1996**, *118*, 12376. (c) Slaughter, L. M.; Wolczanski, P. T. *Chem. Commun.* **1997**, 2109. (d) Glaser, T.; Kesting, F.; Beissel, T.; Bill, E.; Weyhermüller, T.; Klauke, W.; Wieghardt, K. *Inorg. Chem.* **1999**, *38*, 722. (e) Akine, S.; Taniguchi, T.; Nabeshima, T. *Inorg. Chem.* **2008**, *47*, 3255. (f) Greenwood, B. P.; Forman, S. I.; Rowe, G. T.; Chen, C.-H.; Foxman, B. M.; Thomas, C. M. *Inorg. Chem.* **2009**, *48*, 6251. (g) Thomas, C. M. *Comm. Inorg. Chem.* **2011**, *32*, 14. (h) Rudd, P. A.; Liu, S.; Gagliardi, L.; Young, V. G., Jr.; Lu, C. C. *J. Am. Chem. Soc.* **2011**, *133*, 20724.

(12) Zhao, Q.; Betley, T. A. *Angew. Chem., Int. Ed.* **2011**, *50*, 709.

(13) Eames, E. V.; Harris, T. D.; Betley, T. A. *Chem. Sci.* **2012**, *3*, 407.

(14) Eames, E. V.; Betley, T. A. *Inorg. Chem.* **2012**, *51*, 10274.

(15) Wilkinson, G. *Org. Synth.* **1956**, *36*, 31.

(16) Compound 2: $C_{90}H_{88}Fe_7N_{12}C_{14}O_2 \cdot 1.25(C_6H_6)$, $M_r = 2171.95$, triclinic, $P\bar{1}$, $a = 12.761(3)$, $b = 13.232(3)$, $c = 15.826(4)$ Å, $\alpha = 79.669(5)^\circ$, $\beta = 74.646(5)^\circ$, $\gamma = 79.387(5)^\circ$, $V = 2508.9(10)$ Å³, $Z = 1$, $\rho_{\text{calcd}} = 1.438$ Mg/m³, $\mu = 1.147$ mm⁻¹, $R1 = 0.0698$, $wR2 = 0.1983$. Compound 3: $C_{90}H_{88}Fe_6CoN_{12}C_{14}O_2 \cdot 1.25(C_6H_6)$, $M_r = 2175.03$, triclinic, $P\bar{1}$, $a = 12.761(3)$, $b = 13.232(3)$, $c = 15.826(4)$ Å, $\alpha = 79.669(5)^\circ$, $\beta = 74.646(5)^\circ$, $\gamma = 79.387(5)^\circ$, $V = 2508.9(10)$ Å³, $Z = 1$, $\rho_{\text{calcd}} = 1.440$ Mg/m³, $\mu = 1.168$ mm⁻¹, $R1 = 0.0709$, $wR2 = 0.1588$. Compound 4: $C_{43}H_{39}Fe_2CoN_7Cl \cdot 1.5(C_2H_3N)$, $M_r = 1842.95$, triclinic, $P\bar{1}$, $a = 12.754(1)$, $b = 18.156(2)$, $c = 19.233(2)$ Å, $\alpha = 72.238(1)^\circ$, $\beta = 86.489(1)^\circ$, $\gamma = 76.050(1)^\circ$, $V = 4115.8(6)$ Å³, $Z = 2$, $\rho_{\text{calcd}} = 1.487$ Mg/m³, $\mu = 1.204$ mm⁻¹, $R1 = 0.0413$, $wR2 = 0.1007$. Compound 5: $C_{43}H_{39}FeCo_2N_7Cl \cdot 1.5(C_2H_3N)$, $M_r = 1849.11$, triclinic, $P\bar{1}$, $a = 11.183(1)$, $b = 11.844(1)$, $c = 17.588(2)$ Å, $\alpha = 73.418(1)^\circ$, $\beta = 82.232(1)^\circ$, $\gamma = 67.098(1)^\circ$, $V = 2055.8(3)$ Å³, $Z = 1$, $\rho_{\text{calcd}} = 1.494$ Mg/m³, $\mu = 1.256$ mm⁻¹, $R1 = 0.0411$, $wR2 = 0.0948$. Compound 6: $C_{82}H_{72}Fe_2Co_4N_{12}C_{12} \cdot 9.5(C_6H_6)$, $M_r = 2385.86$, triclinic, $P\bar{1}$, $a = 18.084(1)$, $b = 19.073(1)$, $c = 19.329(1)$ Å, $\alpha = 74.288(1)^\circ$, $\beta = 67.149(1)^\circ$, $\gamma = 80.502(1)^\circ$, $V = 5900.6(5)$ Å³, $Z = 2$, $\rho_{\text{calcd}} = 1.343$ Mg/m³, $\mu = 0.891$ mm⁻¹, $R1 = 0.1010$, $wR2 = 0.2914$. CCDC-894769 (2), 894770 (3), 894771 (4), 894772 (5), 894773 (6) contain the supplementary crystallographic data for this paper. These data can be obtained free of charge from the Cambridge Crystallographic Data Centre via www.ccdc.cam.ac.uk/data_request/cif.

(17) Pokhodnya, K. I.; Bonner, M.; DiPasquale, A. G.; Rheingold, A. L.; Her, J.-H.; Stephens, P. W.; Park, J.-W.; Kennon, B. S.; Arif, A. M.; Miller, J. S. *Inorg. Chem.* **2007**, *46*, 2471.

(18) (a) Balch, A. L.; Holm, R. H. *J. Am. Chem. Soc.* **1966**, *88*, 5201. (b) Warren, L. F. *Inorg. Chem.* **1977**, *16*, 2814. (c) Chaudhuri, P.; Verani, C. N.; Bill, E.; Bothe, E.; Weyhermüller, T.; Wieghardt, K. *J. Am. Chem. Soc.* **2001**, *123*, 2213. (d) Anillo, A.; Diaz, M. R.; Garcia-Granda, S.; Obeso-Rosete, R.; Galindo, A.; Ienco, A.; Mealli, C. *Organometallics* **2004**, *23*, 471. (d) Bill, E.; Bothe, E.; Chaudhuri, P.; Chlopek, K.; Herebian, K.; Kokatam, S.; Ray, K.; Weyhermüller, T.; Neese, F.; Wieghardt, K. *Chem.—Eur. J.* **2005**, *11*, 204. (e) Chlopek, K.; Bill, E.; Weyhermüller, T.; Wieghardt, K. *Inorg. Chem.* **2005**, *44*, 7087.

(19) Borrás-Almenar, J. J.; Clemente-Juan, J. M.; Coronado, E.; Tsukerblat, B. S. *J. Comput. Chem.* **2001**, *22*, 985.